International Journal of
INTELLIGENT SYSTEMS AND APPLICATIONS IN ENGINEERING
ISSN:2147-6799 www.ijisae.org Original Research Paper

Glioma Tumor Segmentation from Multi-Modal MRI Images Using Deep Residual and Inception U-Nets

K. Sambath Kumar[1*],T.Latha Maheswari[2], E. Keerthika[3], T. Karthikeyan[4], G.Merlin Suba[5]

Submitted: 19/01/2024 **Revised**: 28/02/2024 **Accepted**: 05/03/2024

Abstract: A glioma is a primary brain tumor that develops within the brain's tissue. It originates from glial cells and keeps neuron in a specific place for normal brain function. Glioma affects all age people, mostly men than women. However, manually segmenting gliomas is a laborious and error-prone task. Recently, researchers working on imaging techniques along with recent deep neural networks (DNN) to segment tumor from the brain tissue. DNN generates features from images without feature engineering procedure. It is a popular technique, especially in medical imaging fields like precise segmentation, image classification and etc. By implementing early treatment strategies, it is possible to improve survival rates and reduce computational time. The main problems with automatic DNN models are bias toward a specific class, imbalanced data, local and global contexts, large training parameters, and accuracy. This research paper analyzes 2D multi-modal magnetic resonance imaging (MRI) image sequences to differentiate between tumor regions and normal brain regions. These models consist of two U-Net topologies for glioma tumor segmentation. The first U-Net incorporates an innovative inception structure design, which leads to exceptional segmentation performance for the whole tumor (WT). The inception structure gathers multi-scale feature maps from various kernels and concatenation layer. On the other hand, the second U-Net tackles degradation problems and reduces training errors, making optimization less complex compared to conventional DNNs. The two-path residual network captures crucial information. In terms of performance and accuracy, the proposed models surpass state-of-the-art models. The high-performance models give great contribution to researchers and physicians for computer vision applications.

Keywords: *Glioma, Brain Tumor, Deep Learning, Segmentation, U-Net, Inception, Rresidual*

1. Introduction

Glioma, composed of star-shaped astrocyte cells, is a highly dangerous brain tumor with a survival rate ranging from a few months to 15 years. Gliomas are categorized into four classes (I–IV) depending on their malignancy by the World Health Organization [1]. Grade II and III gliomas form low-grade gliomas (LGG), whereas grade IV gliomas denote high-grade gliomas (HGG). The most perilous form of primary glioma is glioblastoma, which is grade IV gliomas [2]. Surgery can be used to treat grade I gliomas, which proliferate slowly [3]. In contrast, glioblastoma has a mean survival rate of just 15 months, making it the deadliest grade of glioma. Standard treatments for brain tumor diseases include chemotherapy, radiation therapy, and surgery. Medical experts consider factors such as tumor location, patient age, health status, and tumor sub-region mass to provide suitable treatment plans. The entire tumor is unable to be eliminated due to the deep penetration of the tumor and the intricate anatomy of the brain. The most commonly used diagnostic technique regarding brain scans is magnetic resonance imaging (MRI), which offers more accurate soft tissue and organ images than computed tomography (CT). By generating excellent 3D images, the MRI technique offers a non-invasive way to diagnose brain problems. However, it is common for MR images to contain artifacts and noise caused by various imaging protocols and tools. Therefore, removing these non-brain images enhances the overall accuracy and effectiveness of the diagnosis.

A DNN is crucial in the healthcare industry, as it enables medical professionals to provide advanced care with their support [4–6]. Modern computer-aided diagnostics suppresses errors and produces better results. The deep convolutional neural network (DCNN) successfully generates high sensitivity and specificity scores from the chest X-ray dataset [7]. Compared to U-Net [8], the notable design SDU-Net (stacked dilated convolution U-Net) offers a larger receptive area and a larger number of stages which results superior classification outcomes [9]. The intelligent medical image architecture detects mass, shape, and localization abnormalities [10]. Remote-sensing achieves data segmentation through ResUNet, which leverages various dice loss configurations using the ISPRS Potsdam dataset. The ResUNet model's residual block enhances performance by concatenating multiple atrous convolutions [11]. Furthermore, the SegNet architecture demonstrates improved semantic segmentation performance in both indoor and outdoor scenes [12]. The RDM-Net achieved excellent segmentation in the brain tumor challenge. Deep residual dilate network utilizes a residual-dilated block to improve the performance [13]. The dual U-Net

[1]*Assistant Professor, Department of Electronics and Communication Engineering, Vel Tech Rangarajan Dr Sagunthala R&D Institute of Science and Technology, Avadi, Chennai-600062, Tamil Nadu, India. India. Email: samelectronics.kpm@gmail.com**

[2]*Associate Professor, Department of Computer Science and Engineering, Sri Krishna College of Engineering and Technology, Coimbatore. Tamil Nadu, India. Email: lathamaheswari@skcet.ac.in*

[3]*Assistant Professor, Department of Biomedical Engineering, P.S.R. Engineering College, Sevalpatti, Sivakasi, Tamil Nadu -626140, India. Email: keerthika@psr.edu.in*

[4]*Department of Information Technology, University of Technology and Applied Sciences - Salalah, Sultanate of Oman., Email: karthik.rt@gmail.com*

[5]*Assistant Professor, Department of Electrical and Electronics Engineering, Panimalar Engineering College, Chennai-600123, India. Email: merlinsubag@gmail.com*

architecture combines elements from two distinct U-Net frameworks. The first U-Net collects context data using the pre-trained VGG-19 encoder architecture and atrous spatial pyramid pooling (ASPP). The 2015 MICCAI sub-challenge evaluates the ability to identify polyps, skin lesions, and nuclei [14]. Meanwhile, six tissues of the optic nerve head are separated using a dilated residual U-Net (DRUNET). The identity layer 1x1 of the residual block reduces the dimensionality. Additionally, various dilation rates are employed to transfer attributes from the encoder to the decoder structure and take advantage of contextual information [15].

Pre-processing techniques eliminate unwanted noise caused by magnetic fields. The N4ITK bias-correction method adjusts the image variance of each MRI sequence [34] [16, 17]. Some methodologies excluded zero-pixel-dominated slices to achieve optimal performance [18]. The top and bottom anomalies, which develop 1% of the data, are eliminated by the CNN model to improve the segmentation outcome. Data augmentation techniques achieved superior results [19]. The 3D-Fully CNN approach employs a conditional random field (CRF) with connected component assessment (CCA) to improve the segmentation results. A segmentation network's false positive score is decreased effectively by the CRF-CCA subsequent step. Additional threshold methods improve the hard-examples performance [20]. A completely interconnected CRF approach is used for intrinsic segmentation, showing encouraging results [21]. Lastly, the CNN architecture incorporates a volumetric constraint to eliminate error clusters.

2. Literature review

A bottom residual net along with a deep V-Net create the DSSE-V-Net. The squeeze and excite blocks generate the best suitable activation map using various parameters. The DSSE-V-Net reduces overfitting and converges faster using a deep supervision area [22]. The prediction stage extracts 192 clipped inputs from the brain image. With multi-class dice loss functions, the reliable CNN technique has reduced patching dimensions [23]. The context accumulation path of the CNN-adopted U-Net acquired an input abstraction, while the localization route stored the key features. The decoder's conjunction stages eliminate certain map functions. There are 128×128×128 patches in the training phase. The training performance improves as the batch size increases. For each MRI sequence, the SegNet model was created [24]. Based on the best probability of the class, the SegNet networks generate four characteristic maps, and each of them is classified as edema (ED), enhancing tumor (ET), necrosis or non-enhancing tumor (NCR/NET), or backdrop. The inclusion of a decision tree classification in the SegNet network improves quality. The shrink image removes a portion of the backdrop elements.

The ED, ET, and NCR/NET components comprise the two-path hierarchy design. The top pathway extracts WT, and the bottom pathway classifies four classes using multi-class classifiers. The 38×38×38 patch successfully fixes the class unbalance problem, and densely connected blocks boost performance even more [25]. The most recent models evaluate the Brain Tumor Segmentation Challenge (BraTS) 2017 dataset [26][35]. However, the existing literature had some flaws. The CNN-based U-Net model gives poor results due to its smaller batch size; the DSSE-V-Net model does not perform well due to its narrow receptive field; and the SegNet model struggles because it discards 1% of the greatest and lowest values. The two-route pathway is unable to record dependency histories due to the patch-wise learning strategy. The new models, inception-based U-Net (IMU-Net) and upgraded residue U-Net (RU-Net) deal with such problems.

3. Proposed work

This section provides explanation of proposed methodology. It includes dataset selection, pre-processing techniques, proposed DNN model and post-processing techniques. The following are the centrepieces of the provided work:

- The multi-modal 2D MRI sequences converge faster with undesirable MRI image slices.
- The convolved residual (CR) block converges rapidly and captures fine-grained attributes.
- The modified inception (MI) unit collects multi-parametric feature maps while minimizing over-fitting concerns.

3.1 Dataset selection

The dataset has 210 HGG and 75 LGG volumes. The dataset's images have been interpolated and skull-stripped to a resolution of 1 mm3. The pre-operative multi-institutional MRI scan images contain LGG and HGG volumes. Each volume includes the image modalities T1w, T2w, T1Gd, and Flair. The presence of cerebrospinal fluid (CSF) differentiates T1w and T2w MR images. The CSF is whitish and opaque in T1w and T2w imaging scans. The gadolinium compound can distinguish active lesions from healthy tissue. White matter abnormalities are sensitively picked up by the Flair MRI modality, which mutes the CSF signal. The dataset contains information labelled "1" as NCR or NET, "2" as ED, "4" as ET, and "0" as miscellaneous. Glioma sub-regions are made up of several labels, which are represented as $Y^{WT} = Y^{NCR/NET} + Y^{ED} + Y^{ET}$, Y^{ET} and $Y^{TC} = Y^{NCR/NET} + Y^{ET}$.

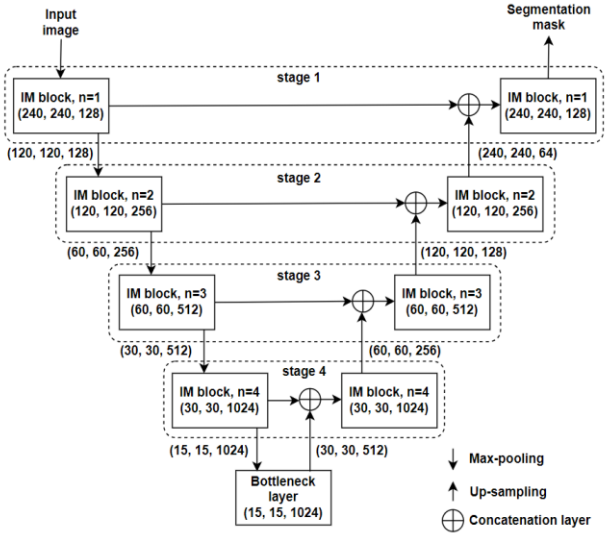

Fig.1 Architecture of IMU-Net

3.2 Pre-processing

T1w, T2w, Flair, and T1Gd MRI images are input for the proposed IMU-Net, whereas any two MRI sequences are input for the designated task for the RU-Net. Both DNN models supplied data using improved N3 bias correction, data standardization, and augmentation procedures. The improved N3 bias correction method eliminates the intensity gradient in raw images. The bias-corrected images show significant standard deviations and the same scale of intensities. Intensity

normalization produces a narrower spectrum of data with a mean close to zero and a standard variation around one [27]. The Z-score standardization is an improved solution for healthcare imaging, which must cope with anomalies. MRI data is rescaled across all modalities. The image augmentation process increases the number of images in the model, expands it, and prevents overfitting [28]. Augmentation techniques, including flipping direction, whirl, elasticity evolve, movement, change, compression, and magnification, are used in the proposed models.

3.3 Deep Neural Networks

Fig. 1 shows the segmentation of the WT using the proposed IMU-Net design [29], whereas Fig. 2 shows the segmentation of the TC and ET using the proposed RU-Net architecture [17]. Both networks use different modules incorporated into the well-known U-Net architecture. There is a bottleneck layer and four encoder-decoder stages in both deep DNNs. The IMU-Net aggregates broad context and intermediate-level features. The inception framework is more complicated than the conventional U-Net architecture. Fine local features and context data are both captured by RU-Net. The residual connections outperform the gradient data with regard to growth.

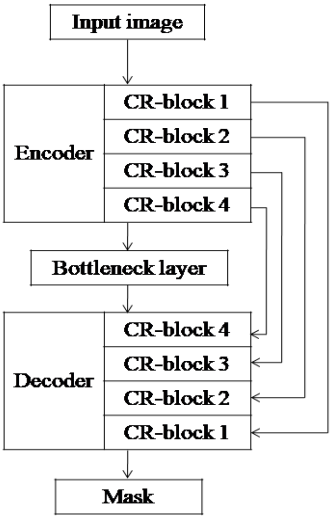

Fig.2 Architecture of RU-Net

Both networks have an encoder path with a down-sampling layer and an IM-unit or CR-block, and a decoder path with an IM-unit or CR-block, upward sampling, and concatenated layers. Fig. 3 and Fig. 4 show the basic functional blocks IM-unit and CR-block for the encoder-decoder structure. The IM-unit has triple path of 5×5, 3×3 and 1×1 convolution kernels to collect multi-scale features. The CR-block has residual path for faster converges. For encoder routes, the channel count is doubled while the spatial dimension is reduced by a factor of two. The decoder pathways lower the total number of channels by half while increasing the dimension of space by a factor of two. The addition step improves learning precision. The output of the concatenation layer is sent into the prior-stage upsampling layer, as well as the necessary coder output. With fine-grained features, the concatenation result produces high-resolution images. The top layer makes a distinction between the tumor and uninterested regions.

3.4 Post-processing

By reducing false-positive scores, the CRF post-processing technique enhances the predicted pattern's performance even more. Misclassified labels are removed from the predicted pattern using the CRF approach.

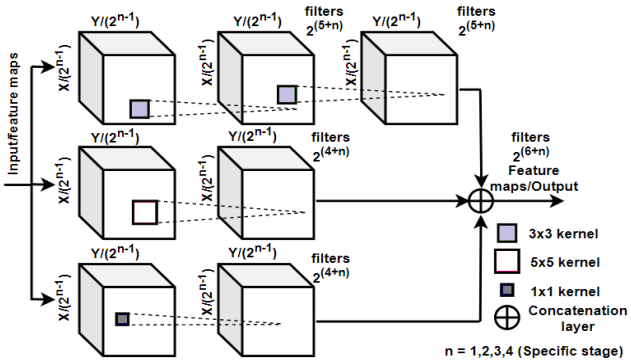

Fig.3 The basic structure of IM-unit

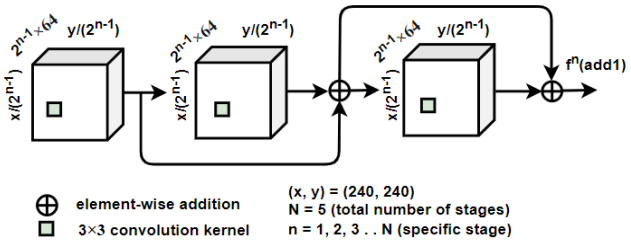

Fig.4 The basic structure of CR-block

4. Results and Discussion

This section comprises the experimentation on the proposed methodology. It also describes the selection of evaluation metrics and performance comparison with state-of-the-art methods.

4.1 Model Configuration

The proposed DNN architectures employ the dice similarity coefficient (DSC) as a measure of performance, the dice-loss cost function, and Adam as an optimizer function. DSC is the preferred statistical metric in the MICCAI competitions for segmentation challenges. It works better for medical images, which have a lot of background pixels [30, 31]. The scale ranges from 0 (no matching samples) to 1 (a perfect match); it assesses the resemblance between two data points. The assessment of DSC is illustrated by Equation (1), wherein X_i is the actual data item and Y_i is the anticipated example. A differentiable dice loss handles the imbalanced datasets efficiently. It calculates the discrepancy between the anticipated samples and the actual samples.

$$\mathrm{DSC} = \frac{2(X_i \cap Y_i)}{X_i + Y_i} \tag{1}$$

The Adam method optimizes the gradients of the model parameters. It is effective for models with a large number of parameters or limited information [32]. It added the benefits of the root mean square propagation (RMSP) and momentum approaches. When model parameters are modified, the learning rate changes. The aforementioned qualities need less memory and reach global minima sooner. The Adam optimizer first sets the

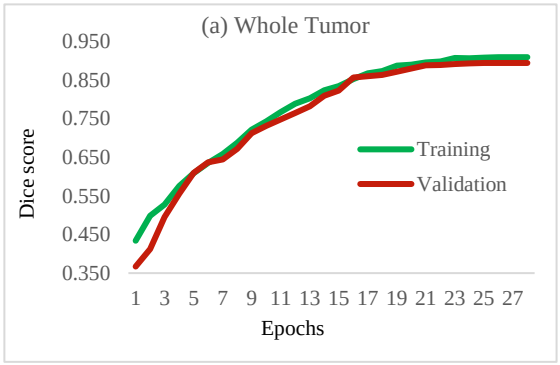

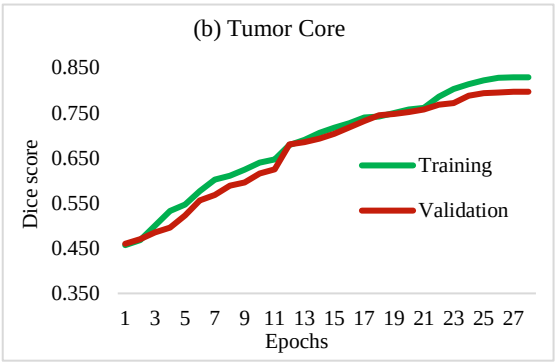

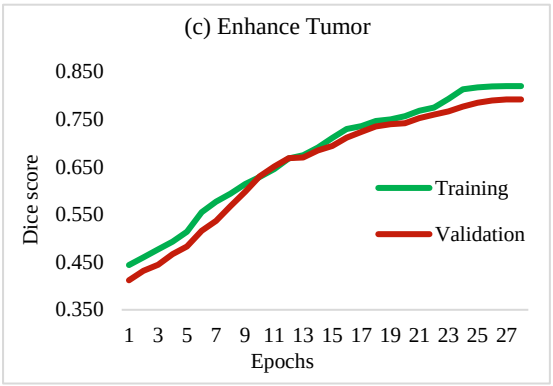

Fig.5 Dice score of (a) WT (b) TC (c) ET vs epochs of the proposed DNN models

following parameters: the adaptive learning rate (η) is 30e-05, the rate of loss of the first inertia (β_1) is 9e-1, the rate of loss of the second inertia (β_2) is 9.99e-1, and ξ is 1e-08 to rapidly converge the model. The skewed first inertia (p_t) and skewed second inertia (q_t) are described in Equations (2) and (3). At time t, g_t is a gradient of parameter w.

$$p_t = \beta_1 p_{t-1} + (1-\beta_1) g_t \quad (2)$$

$$q_t = \beta_2 q_{t-1} + (1-\beta_2) g_t^2 \quad (3)$$

Equations (4) and (5) are used to determine the skewed-corrected first and second inertia.

$$\hat{p}_t = \frac{p_t}{1-\beta_1^t} \quad (4)$$

$$\hat{q}_t = \frac{q_t}{1-\beta_2^t} \quad (5)$$

Equation (6) contains the parameter updating rule for the Adam optimizer.

$$w_t = w_{t-1} - \eta \frac{\hat{p}_t}{\sqrt{\hat{q}_t}+\xi} \quad (6)$$

where w_{t-1} denotes the preceding parameter matrix. The relu non-linear activity function generates an improved non-linear framework and solves the vanishing gradient issue. The sigmoid activation function differentiates the background and tumor sub-regions in the classification layer.

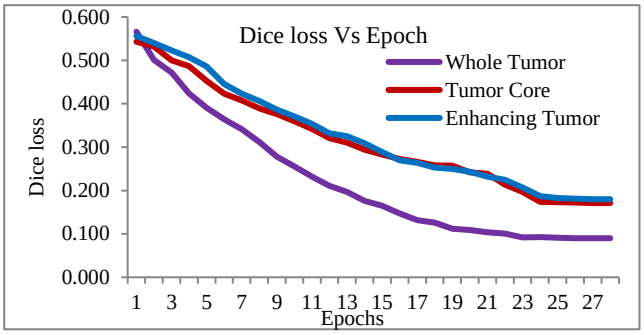

Fig.6 Dice loss vs epochs of the proposed DNN models

4.2 Experimentation

IMU-Net extracts WT from the four MRI sequences. According to the RU-Net, the T1Gd and Flair MRI sequences partition the region known as the ET, whereas the T1Gd and T2w sequences split the TC. For evaluation reasons, WT comprises NCR/NET sub-regions in addition to TC, which covers ET and ED. The actual input dimensions are fed into the model, where 2402 refers to the 2-dimensional data of an input. The proposed method only employs MRI image slices from 51 to 110 due to the predominance of background pixels; all other slices are eliminated. The random data divides training and validation data into two partitions of 80:20.

The N4ITK approach removes non-uniformity from the data. The Z-score standardization transforms unnormalized data into normalized data. From a single sample, the data augmentation technique generates eight alternative samples. Finally, there are 437760 images in the training data for the WT task, and 328320 images in the training data for the ET and TC tasks. The CRF method avoids false negatives and effectively classifies labels in order to find patterns. To cut down on computational costs, the suggested models acquire data in batches, with each including 16 images. The suggested methods implement the TensorFlow framework, the TensorLayer deep learning library[36], and the NVIDIA DGX-1 cluster [33].

Table 1 Comparison of evaluation results with existing methods

Methods	*Input*	*DSC*		
		WT	*TC*	*ET*
SegNet [24]	192×192×3	0.84	0.8	0.79
U-Net [23]	128×128×128	0.86	0.75	0.65
DSSE-V-Net [22]	128×128×128	0.88	0.78	0.71
Two-pathway [25]	38×38×38	0.73	0.83	0.8
Proposed IMU-Net	240×240×4	0.91	-	-
Proposed RU-Net	240×240×2	-	0.8	0.82

4.3 Comparison with state-of-the-art methods

The proposed IMU-Net extracts deep features from four different MRI modalities and creates patterns for all sub-regions to make WT. The MI-unit captured multi-scale features such as low-, middle-, and high-level features. Another advantage of the MI-

unit is that it reduces dimensionality over the U-Net structure. Through identical information flow through all layers, the proposed RU-Net converges quickly. The use of multi-modality MRI sequences in conjunction with 2D slices reduces computational costs. Fig. 5 displays the efficacy study for the presented approaches, with dice scores and epochs provided for all tumor regions. The 5-fold cross-validation improves the model's generalization. The validation process strengthens the model's accuracy even more. The dice loss optimizes the proposed framework with different parameter configurations. Fig. 6 depicts the dice loss during the training stage for each tumor region. During the training step, the dice loss decreases with each epoch, validating the proposed model in terms of reliability.

U-Net and modified V-Net applied convolution kernels made up of 128×128×128 patches with modest batch sizes. These architectures can't be used to collect every tumor sub-region. The SegNet models require a significant amount of training time and training variables. The maximal feature map approach, however, is unable to more accurately predict WT. The two-pathway architecture, which combines two small patches, is insufficient to forecast the WT pattern. The majority of modern models use patch-wise training to accelerate computation, although this results in redundant data. To overcome these limitations, the proposed methods concentrate on the full-sized 240×240 image. In addition, the 60 slices of 2D MRI images lower the computational cost. Depending on the tumor area, the proposed models incorporate particular MRI modalities. During the training phase, the adaptive gradient modifies the model's parameters and produces a well-fit model. The CRF post-processing method also accurately categorizes tumor sub-regions and backdrops. Table 1 compares the performance of the proposed model to that of cutting-edge models. Fig. 7 shows the visual comparison of proposed method with existing methods. From the Fig.7 and Table 1, the proposed models are the most successful segmentation approaches when compared to modern algorithms for the WT and ET regions. The TC zone, on the other hand, is where the two-pathway model achieves the greatest accuracy. The small patch methodology tries to extract depth features to segment TC and ET regions effectively rather than WT region.

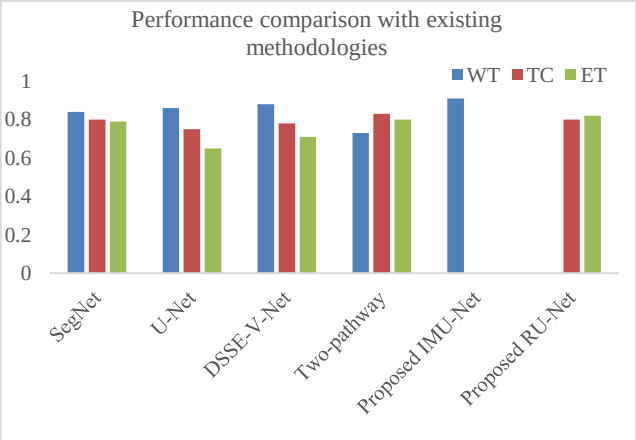

Fig.7 Performance comparison with existing methodologies

5. Conclusion and future work

The proposed segmentation architectures use deep layers to collect contextual and fine-grained details. MI-unit generates multi-scale features using different kernels. The CR-block creates regional context information, overcomes gradient loss difficulties, and facilitates faster convergence. In the CR-block, the pixel-wise addition layer uses less processing power and memory than the concatenation layer. The suggested models outperform segmentation scores and acquire low- to high-level feature maps. In contrast, the proposed approach employs fewer training parameters than current deep segmentation networks. Finally, the proposed DNN models provide high accuracy and low computation. By incorporating different modules into the proposed architecture or changing the arrangement of modules, the segmentation of TC will be improved.

References

[1] Comprehensive, Integrative Genomic Analysis of Diffuse Lower-Grade Gliomas. (2015). New England Journal of Medicine, 372(26), 2481–2498. https://doi.org/10.1056/nejmoa1402121.

[2] Hanif, F., Muzaffar, K., Perveen, K., Malhi, S. M., & Simjee, S. U. (2017). Glioblastoma multiforme: A review of its epidemiology and pathogenesis through clinical presentation and treatment. Asian Pacific Journal of Cancer Prevention, 18(1), 3–9. https://doi.org/10.22034/APJCP.2017.18.1.3.

[3] Dugdale, E., & Gerrard, G. (2006). Low-grade gliomas in adults. CME Cancer Medicine, 3(3), 40–45. https://doi.org/10.3171/2011.7.jns10238.

[4] Venkataramanaiah, B., Sambath Kumar, K., & Giridhar Reddy, K. (2023). Brain Disorders Identification by Machine Learning Classifiers. Journal of Physics: Conference Series, 2466(1). https://doi.org/10.1088/1742-6596/2466/1/012036

[5] Venkataramanaiah, B., & Kamala, J. (2020). ECG signal processing and KNN classifier-based abnormality detection by VH-doctor for remote cardiac healthcare monitoring. Soft Computing, 24(22), 17457–17466. https://doi.org/10.1007/s00500-020-05191-1.

[6] Kumar, K. S., & Rajendran, A. (2021). Machine Learning Classifiers in Health Care. In Machine Learning and Analytics in Healthcare Systems. https://doi.org/10.1201/9781003185246-5

[7] Pereira, S., Pinto, A., Alves, V., & Silva, C. A. (2016). Brain Tumor Segmentation Using Convolutional Neural Networks in MRI Images. IEEE Transactions on Medical Imaging, 35(5), 1240–1251. https://doi.org/10.1109/TMI.2016.2538465.

[8] Navab, N., Hornegger, J., Wells, W. M., & Frangi, A. F. (2015). Medical Image Computing and Computer-Assisted Intervention - MICCAI 2015: 18th International Conference Munich, Germany, October 5-9, 2015 proceedings, part III. Lecture Notes in Computer Science (including subseries Lecture Notes in Artificial Intelligence and Lecture Notes in Bioinformatics), 9351(Cvd), 12–20. https://doi.org/10.1007/978-3-319-24574-4.

[9] Wang, S., Hu, S.-Y., Cheah, E., Wang, X., Wang, J., Chen, L., … Samir, A. (2020). U-Net Using Stacked Dilated Convolutions for Medical Image Segmentation. Retrieved from http://arxiv.org/abs/2004.03466.

[10] Sarvamangala, D. R., & Kulkarni, R. V. (2021). Convolutional neural networks in medical image understanding: a survey. Evolutionary Intelligence, (0123456789). https://doi.org/10.1007/s12065-020-00540-3.

[11] Diakogiannis, F. I., Waldner, F., Caccetta, P., & Wu, C. (2020). ResUNet-a: A deep learning framework for semantic segmentation of remotely sensed data. ISPRS Journal of Photogrammetry and Remote Sensing, 162, 94–114. https://doi.org/10.1016/j.isprsjprs.2020.01.013.

[12] Badrinarayanan, V., Kendall, A., & Cipolla, R. (2017). SegNet: A Deep Convolutional Encoder-Decoder Architecture for Image Segmentation. IEEE Transactions on Pattern Analysis and Machine Intelligence, 39(12), 2481–2495. https://doi.org/10.1109/TPAMI.2016.2644615.

[13] Ding, Y., Li, C., Yang, Q., Qin, Z., & Qin, Z. (2019). How to Improve the Deep Residual Network to Segment Multi-Modal Brain Tumor Images. IEEE Access, 7, 152821–152831. https://doi.org/10.1109/ACCESS.2019.2948120.

[14] Jha, D., Riegler, M. A., Johansen, D., Halvorsen, P., & Johansen, H. D. (2020). DoubleU-Net: A deep convolutional neural network for medical image segmentation. Proceedings - IEEE Symposium on Computer-Based Medical Systems, 2020-July(1), 558–564. https://doi.org/10.1109/CBMS49503.2020.00111.

[15] Devalla, S. K., Renukanand, P. K., Sreedhar, B. K., Subramanian, G., Zhang, L., Perera, S., … Girard, M. J. A. (2018). DRUNET: a dilated-residual U-Net deep learning network to segment optic nerve head tissues in optical coherence tomography images. Biomedical Optics Express, 9(7), 3244. https://doi.org/10.1364/boe.9.003244.

[16] Noori, M., Bahri, A., & Mohammadi, K. (2019). Attention-guided version of 2D UNet for automatic brain tumor segmentation. 2019 9th International Conference on Computer and Knowledge Engineering, ICCKE 2019, 269–275. https://doi.org/10.1109/ICCKE48569.2019.8964956.

[17] Kumar, K. S., & Rajendran, A. (2023). Deep Convolutional Neural Network for Brain Tumor Segmentation. Journal of Electrical Engineering and Technology. https://doi.org/10.1007/s42835-023-01479-y.

[18] Awasthi, N., Pardasani, R., & Gupta, S. (2021). Multi-threshold Attention U-Net (MTAU) Based Model for Multimodal Brain Tumor Segmentation in MRI Scans. Lecture Notes in Computer Science (including subseries Lecture Notes in Artificial Intelligence and Lecture Notes in Bioinformatics), 12659 LNCS, 168–178. https://doi.org/10.1007/978-3-030-72087-2_15.

[19] Yadav, S. S., & Jadhav, S. M. (2019). Deep convolutional neural network based medical image classification for disease diagnosis. Journal of Big Data, 6(1). https://doi.org/10.1186/s40537-019-0276-2.

[20] Anand, V. K., Grampurohit, S., Aurangabadkar, P., Kori, A., Khened, M., Bhat, R. S., & Krishnamurthi, G. (2021). Brain Tumor Segmentation and Survival Prediction Using Automatic Hard Mining in 3D CNN Architecture. Lecture Notes in Computer Science (including subseries Lecture Notes in Artificial Intelligence and Lecture Notes in Bioinformatics), 12659 LNCS, 310–319. https://doi.org/10.1007/978-3-030-72087-2_27.

[21] Zhou, Z., He, Z., & Jia, Y. (2020). AFPNet: A 3D fully convolutional neural network with atrous-convolution feature pyramid for brain tumor segmentation via MRI images. Neurocomputing, 402, 235–244. https://doi.org/10.1016/j.neucom.2020.03.097.

[22] Liu, P., Dou, Q., Wang, Q., & Heng, P. A. (2020). An encoder-decoder neural network with 3D squeeze-and-excitation and deep supervision for brain tumor segmentation. IEEE Access, 8, 34029–34037. https://doi.org/10.1109/ACCESS.2020.2973707

[23] Isensee, F., Kickingereder, P., Wick, W., Bendszus, M., & Maier-hein, K. H. (2017). Brain Tumor Segmentation and Radiomics Survival Prediction: Contribution to the BRATS 2017 Challenge.

[24] Alqazzaz, S. (2019). Automated brain tumor segmentation on multi-modal MR image using SegNet, 5(2), 209–219.

[25] Chen, L., Wu, Y., Dsouza, A. M., Abidin, A. Z., & Wism, A. (n.d.). MRI Tumor Segmentation with Densely Connected 3D CNN.

[26] Menze, B. H., Jakab, A., Bauer, S., Kalpathy-Cramer, J., Farahani, K., Kirby, J., … Van Leemput, K. (2015). The Multimodal Brain Tumor Image Segmentation Benchmark (BRATS). IEEE Transactions on Medical Imaging, 34(10), 1993–2024. https://doi.org/10.1109/TMI.2014.2377694.

[27] Shalabi, L. Al, Shaaban, Z., & Kasasbeh, B. (2006). Data Mining: A Preprocessing Engine. Journal of Computer Science, 2(9), 735–739. https://doi.org/10.3844/jcssp.2006.735.739.

[28] Shorten, C., & Khoshgoftaar, T. M. (2019). A survey on Image Data Augmentation for Deep Learning. Journal of Big Data, 6(1). https://doi.org/10.1186/s40537-019-0197-0.

[29] Sambath Kumar, K., & Rajendran, A. (2021). An automatic brain tumor segmentation using modified inception module based U-Net model. Journal of Intelligent & Fuzzy Systems, 42(3), 2743–2754. https://doi.org/10.3233/jifs-211879.

[30] Bertels, J., Eelbode, T., Berman, M., Vandermeulen, D., Maes, F., Bisschops, R., & Blaschko, M. B. (2019). Optimizing the Dice Score and Jaccard Index for Medical Image Segmentation: Theory and Practice. Lecture Notes in Computer Science (including subseries Lecture Notes in Artificial Intelligence and Lecture Notes in Bioinformatics), 11765 LNCS, 92–100. https://doi.org/10.1007/978-3-030-32245-8_11.

[31] Bakas, S., Akbari, H., Sotiras, A., Bilello, M., Rozycki, M., Kirby, J. S., … Davatzikos, C. (2017). Advancing The Cancer Genome Atlas glioma MRI collections with expert segmentation labels and radiomic features. Scientific Data, 4(July), 1–13. https://doi.org/10.1038/sdata.2017.117

[32] Kingma, D. P., & Ba, J. L. (2015). Adam: A method for stochastic optimization. 3rd International Conference on Learning Representations, ICLR 2015 - Conference Track Proceedings, 1–15

[33] Dong, H., Supratak, A., Mai, L., Liu, F., Oehmichen, A., Yu, S., & Guo, Y. (2017). TensorLayer: A versatile library for efficient deep learning development. MM 2017 - Proceedings of the 2017 ACM Multimedia Conference, (1), 1201–1204. https://doi.org/10.1145/3123266.3129391.

[34] K. S. Raju, S. Arvind, R. Chegoni, V. A. Naryana, A. Vivekananda and C. R. Kishore Babu, "Assessment of 3D MRI Image segmentation and Classification for Brain Tumor Detection Using ConvLSTM," 2023 IEEE 5th International Conference on Cybernetics, Cognition and Machine Learning Applications (ICCCMLA), Hamburg, Germany, 2023, pp. 665-670, doi: 10.1109/ICCCMLA58983.2023.10346772.

[35] Rinesh, S., K. Maheswari, B. Arthi, P. Sherubha, A. Vijay, S. Sridhar, T. Rajendran, and Yosef Asrat Waji. "Investigations on brain tumor classification using hybrid machine learning algorithms." Journal of Healthcare Engineering 2022 (2022).

[36] Muni, T. Vijay, Ravi Kumar Tata, Jonnadula Narasimharao, K. Murali, and Harpreet Kaur. "Deep Learning Techniques for Speech Emotion Recognition." In *2022 International Conference on Futuristic Technologies (INCOFT)*, pp. 1-5. IEEE, 2022.